ELSEVIER

Solid State Sciences 4 (2002) 973–978

Solid State Sciences

www.elsevier.com/locate/ssscie

A neutron diffraction study of the antiferromagnetic diphosphate $LiFeP_2O_7$

Gwenaëlle Rousse [a,*], Juan Rodríguez-Carvajal [b,c], Calin Wurm [d], Christian Masquelier [d]

[a] *Institut Laue Langevin, BP 156, F-38042 Grenoble cedex 9, France*
[b] *Laboratoire Léon Brillouin (CEA-CNRS), CEA/Saclay, 91191 Gif sur Yvette cedex, France*
[c] *Service de Physique Statistique, CEA/Grenoble, 17 avenue des Martyrs, 38054 Grenoble cedex 9, France*
[d] *Laboratoire de Réactivité et Chimie des Solides, Université Picardie Jules Verne, 33 rue St. Leu, 80039 Amiens cedex 9, France*

Received 4 February 2002; accepted 11 April 2002

Abstract

The magnetic structure of $LiFeP_2O_7$ (monoclinic, space group $P2_1$) has been solved using neutron diffraction on a polycrystalline sample. $LiFeP_2O_7$ presents an antiferromagnetic behaviour below 22 K characterized by a long-range ordering observed in the neutron diffraction patterns below the Néel temperature. The magnetic reflections can be indexed with a propagation vector $\mathbf{k} = (0, 0, 0)$. The magnetic moments of the two iron atoms present in the unit cell are oriented anti-parallel along [1 0 0], with a small component of the magnetic moment along [0 0 1]. The magnetic structure is discussed in terms of super-super exchange interactions involving two oxygen atoms belonging to a PO_4 tetrahedron.

Keywords: Iron diphosphate; Magnetic structure; Neutron diffraction; Li batteries; Super-super exchange interactions

1. Introduction

Compositions with general formula $LiMX_2O_7$ (M = Fe, V; X = P, As) have been subjected to intense research for the past few years, mainly for their interesting crystal chemistry and more recently for their interesting properties as positive electrode materials in lithium rechargeable batteries [1–5]. In these 3-D structures, the transition metal is surrounded by 6 oxygen atoms forming a rather regular octahedron. This transition metal element can be reduced (or oxidized) by insertion (or extraction) of lithium ions in/from the tunnels of the structure. Moreover, these compounds may present interesting magnetic properties, as iron atoms are connected through super-super exchange paths, involving diphosphate groups (made of two corner-sharing PO_4 tetrahedra).

$LiFeP_2O_7$, to which this paper is devoted, is not isostructural with the sodium diphosphate $NaFeP_2O_7$, whose magnetic structure has been widely studied in the early 1990's [6–8]: although both structures content diphosphate groups, one of them chelating the FeO_6 octahedron, the 3-D connectivity is different, leading to different space groups ($P2_1/c$ for $NaFeP_2O_7$, $P2_1$ for $LiFeP_2O_7$) [7–9]. This has been discussed in details by Belkouch et al. [9]. Magnetic studies of $LiFeP_2O_7$ are scarce: to our knowledge, only one paper deals with magnetic properties of this compound [3]. Susceptibility measurements reveal an antiferromagnetic behaviour, with negative paramagnetic Curie temperature ($\theta = -73(5)$ K), and a Néel temperature of $T_N = 22(5)$ K. The number of Bohr magnetons derived from the Curie–Weiss law in the paramagnetic state is found equal to 5.89 μ_B in good agreement with the expected, spin-only ($S = 5/2$), value ($\mu_{eff} = 2\sqrt{S(S+1)} = 5.92\ \mu_B$) for high spin Fe^{3+}. We present here a neutron diffraction study at low temperature, that has been performed in order to detect the presence of magnetic reflections and solve the magnetic structure.

2. Experimental

2.1. Sample preparation

$LiFeP_2O_7$ was prepared from LiH_2PO_4, $NH_4H_2PO_4$ and $Fe(NO_3)_3^{\bullet}9H_2O$, each of them dissolved in de-mineralized

* Correspondence and reprints.
E-mail addresses: rousse@ill.fr (G. Rousse), juan@llb.saclay.cea.fr (J. Rodríguez-Carvajal), calin.wurm@u-picardie.fr (C. Wurm), christian.masquelier@u-picardie.fr (C. Masquelier).

1293-2558/02/$ – see front matter
PII: S1293-2558(02)01347-X

water at concentrations of 1 mol L^{-1}. The pH was adjusted to 6 with the use of NH_4OH. The solutions were slowly mixed together under continuous stirring followed by a slow evaporation to dryness before annealing the resulting solid at temperatures ranging from 300 to 800 °C with intermediate grinding. The solid investigated in this study was obtained after a final treatment of 24 hours at 800 °C. Further details of the synthesis of $LiMX_2O_7$ compositions are described in [5].

2.2. Neutron diffraction

Neutron diffraction experiments were performed on polycrystalline $LiFeP_2O_7$ at the Institute Laue Langevin (ILL, Grenoble, France), on the high intensity powder diffractometers D20 and D1B. Both experiments have been performed with a wavelength of 2.41 Å (D20) or 2.52 Å (D1B) obtained by a HOPG graphite monochromator. The powdered sample was placed inside a vanadium can mounted on a cryostat. D20 has been used to confirm the nuclear structure at 240 K (far above T_N), using only a vertical 10 mm wide window in the centre of the monochromator and 10' primary slits to increase the resolution of the data. D1B has been used in its normal high flux configuration for measuring the sample between 80 and 1.5 K. The program FULLPROF [10] was used for crystal structure refinements using the Rietveld method [11].

3. Results and discussion

3.1. Nuclear structure of $LiFeP_2O_7$

The nuclear structure of $LiFeP_2O_7$ has been investigated using the D20 neutron diffraction data recorded at 240 K ($\lambda = 2.41$ Å). Our refinement was performed using the initial list of atomic positions in the nuclear structure, found by Riou et al. [3], from single crystal X-ray diffraction data. The refinement is in perfect agreement with the published structure (Table 1), and is shown Fig. 1. As the structure has been explained in very much details in Riou's paper, we will just remind some important points: the structure is monoclinic with space group $P2_1$, and all the atoms are distributed in the only possible general position 2*a* (Table 1). There is only a single site for Fe atoms. The Fe atom is located at the middle of an almost regular O_6 octahedron, with Fe–O distances ranging from 1.957(7) to 2.04(1) Å, characteristic of iron in the +III valence state in octahedral co-ordination. Each FeO_6 octahedron is connected to six P_2O_7 groups, one of them being bidentate. Lithium ions are located inside the tunnels defined by diphosphate groups (Fig. 2). These tunnels, and the cavities associated, are at the origin of possible alkali metal migration within the structure and further intercalation of extra alkali cations [5].

Table 1
Unit cell parameters of $LiFeP_2O_7$ determined from neutron diffraction at 1.5 K ($P2_1$). The atomic positions and their *B*'s are those determined by Riou et al. from single crystal X-ray diffraction [3]. Atomic positions of magnetic ions in the unit cell and their magnetic moment (μ_B) at 1.5 K

$LiFeP_2O_7$, D1B ($\lambda = 2.52$ Å) at 1.5 K				
Atom	*x*	*y*	*z*	B_{iso} (Å^2)
Li(1)	0.8030	0.3840	0.8190	2.00
Fe(1)	0.2195	0.25	0.2340	0.387
P(1)	0.7939	0.4704	0.4166	0.406
P(2)	0.6008	0.0709	0.9802	0.368
O(1)	0.4029	0.0722	0.1099	0.680
O(2)	0.8141	0.2156	0.0198	0.610
O(3)	0.1318	0.0616	0.3813	0.700
O(4)	0.0619	0.4302	0.3611	0.840
O(5)	0.2481	0.4056	0.0103	0.580
O(6)	0.3985	0.1016	0.7475	0.730
O(7)	0.6082	0.3197	0.4183	0.780

Magnetic moments (μ_B) at 1.5 K

Atom	*x*	*y*	*z*	M_X	M_Y	M_Z
Fe1	*x*	*y*	*z*	4.84(4)	0	0.9(1)
Fe2	$-x$	$y + 1/2$	$-z$	$-4.84(4)$	0	$-0.9(1)$

Nuclear space group $P2_1$, $a = 4.8091(6)$, $b = 8.0574(9)$, $c = 6.928(1)$, $\beta = 109.379(5)°$. R_p: 6.25, R_{wp}: 6.21, R_{exp}: 1.50, Bragg *R*-factor: 9.45, magnetic *R*-factor: 6.73, $N - P + C$: 303, total number of "independent" reflections: 164.

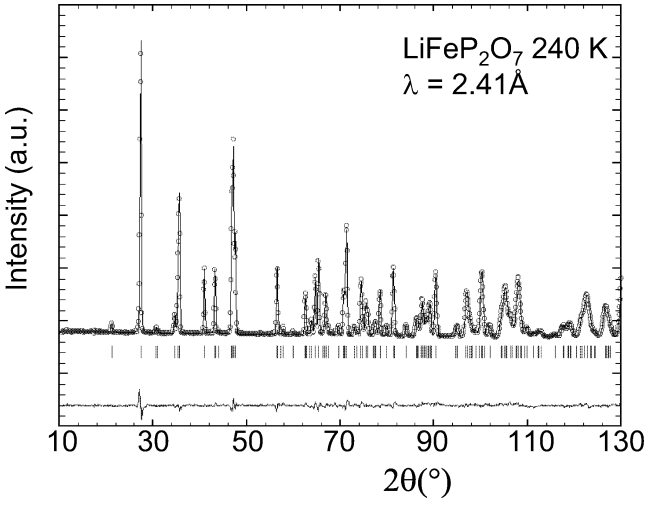

Fig. 1. Calculated (continuous line) and experimental (circles) neutron diffraction patterns of $LiFeP_2O_7$ at 240 K (D20 'high resolution' mode, $\lambda = 2.41$ Å), using the structural model of Riou et al. [3].

3.2. Magnetic structure of $LiFeP_2O_7$

The neutron diffraction patterns collected when $LiFeP_2O_7$ is cooled below T_N show the appearance of some extra reflections (Fig. 3). All these reflections can be indexed with a propagation vector $\mathbf{k} = (0, 0, 0)$, so that the magnetic unit cell is the same as the nuclear one. Fig. 4 presents the evolution of the intensity of the main magnetic reflection, (0 1 0), as a function of temperature. The appearance of the magnetic reflections below 22 K is in perfect agreement with the

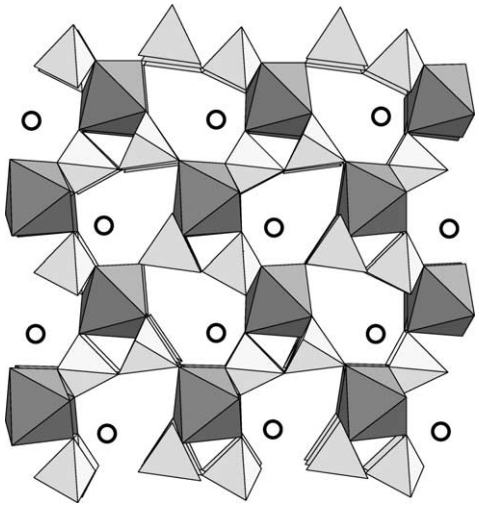

Fig. 2. Structure of $LiFeP_2O_7$. Lithium ions (open circles) are located in tunnels delimited by FeO_6 octahedra and PO_4 tetrahedra.

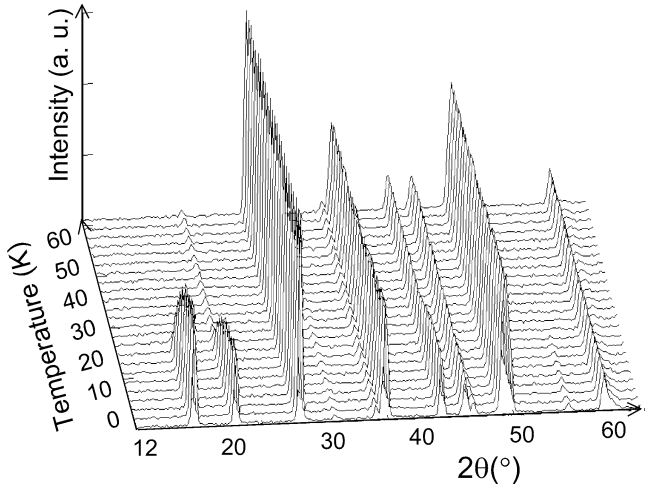

Fig. 3. Neutron diffraction patterns of $LiFeP_2O_7$ (D1B, $\lambda = 2.52$ Å) between 1.5 and 80 K, showing the appearance of magnetic peaks at low temperature.

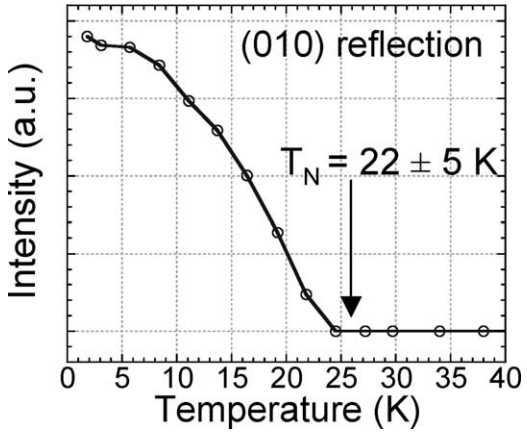

Fig. 4. Evolution of the intensity of the (0 1 0) magnetic reflection as a function of temperature. The value of the Néel temperature, determined from magnetic measurements by Riou et al. [3], is also indicated.

value of the Néel temperature published by Riou et al. [3]. As already pointed out, the 2 magnetic Fe^{3+} ions of the cell are distributed in one crystallographic site, at general position $2a$, with $x \approx 0.219$, $y = 0.25$, $z \approx 0.234$. Note that the coordinates of the iron atom fix the origin along the y axis. We label these two atoms Fe1 and Fe2. Note that for the nuclear part, we used the atomic coordinates published by Riou and confirmed at 240 K on D20, as we do not have enough information with the D1B data (long wavelength of 2.52 Å, low resolution at high 2θ angle) to properly refine both nuclear and magnetic parts: all the position parameters were fixed.

The different possibilities of magnetic configurations were investigated using Bertaut's symmetry analysis method [12,13] that allows to determine the symmetry constraints between each magnetic moment of Fe^{3+} belonging to the same general crystallographic position. The total magnetic representation of the propagation vector group can be decomposed upon 2 irreducible representations, each with 3 basis vectors:

$$\Gamma = 3(\Gamma_1 + \Gamma_2),$$

leading to 2 possible spin configurations:

$$\begin{aligned}
\Gamma_1: \quad & A^X = S_1^X - S_2^X, \qquad F^Y = S_1^Y + S_2^Y, \\
& A^Z = S_1^Z - S_2^Z, \\
\Gamma_2: \quad & F^X = S_1^X + S_2^X, \qquad A^Y = S_1^Y - S_2^Y, \\
& F^Z = S_1^Z + S_2^Z,
\end{aligned}$$

where S_i^X is the component along x of the magnetic moment of atom (i). For example, the representation Γ_1 corresponds to a ferromagnetic coupling of the 2 moments in the y direction (F^Y), whereas in the x and z directions (A^X and A^Z), the moments are coupled antiferromagnetically.

We tried all these magnetic models by least square refinements. Over all the possibilities, the collinear solution $A^X = S_1^X - S_2^X$ (Γ_1), with a moment of 4.60(3) μ_B gives the best agreement between observed and calculated patterns. No component of the magnetic moment exists along y. This is in agreement with the absence of a ferromagnetic component that was not detected by macroscopic measurements [3]. Introducing a component on the z axis (A^Z, Γ_1) gives slightly better reliability factors. The magnetic moment is then refined to 4.84(4) μ_B along x and 0.9(1) μ_B along z, leading to exactly the same total magnetic moment of 4.60(3), slightly lower than the expected value of 5 μ_B for Fe^{3+} in high-spin configuration. Although it is very difficult to distinguish between these two solutions regarding the global agreement factors obtained from the Rietveld refinement, we were able to give a definite answer by looking around the profile of the weak $(1\,0\,0)/(-1\,0\,1)$ reflections. Fig. 5 presents a zoom of the fitted profile using the two collinear models: it is clear that the model with a small component along z gives a better refinement. The final refinement is

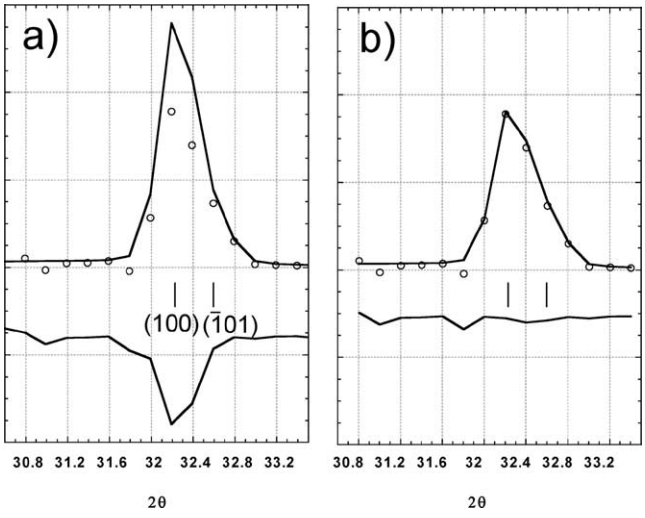

Fig. 5. Zoom around the $(100)/(-101)$ reflections in the Rietveld refinement at 1.5 K, using a collinear model along x (a) or with a component along the z axis (b) for the magnetic part.

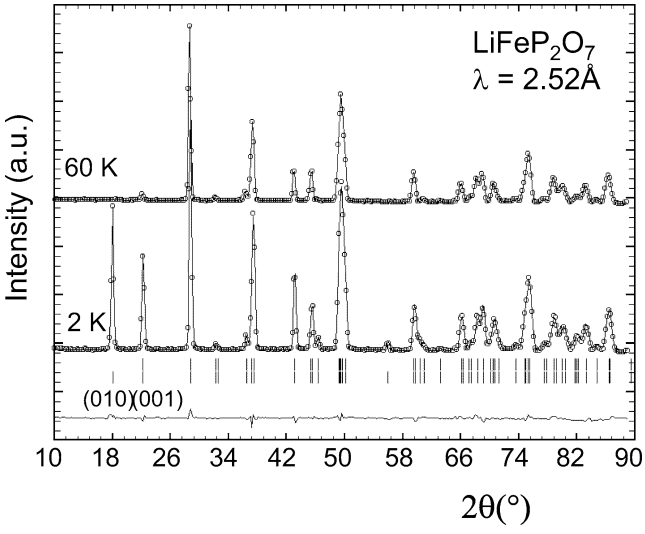

Fig. 6. Observed (circles) versus calculated (continuous line) neutron powder diffraction patterns of $LiFeP_2O_7$ (D1B, $\lambda = 2.52$ Å) at 1.5 K. The positions of the Bragg reflections are represented by vertical bars (first row = nuclear, second row = magnetic). The difference (obs–calc) pattern is displayed at the bottom of the figure. The pattern recorded at 60 K (i.e., above the magnetic transition) is displayed for comparison.

shown in Fig. 6 and the corresponding magnetic structure is shown in Fig. 7. The magnetic moments of Fe atoms within the unit cell are indicated in Table 1, together with unit cell, atomic positions and the reliability factors. A list of calculated and "observed" magnetic interaction vectors squared for each $(h\,k\,l)$ reflection is displayed in Table 2.

3.2.1. Analysis and discussion of the magnetic structure. Magnetic phase diagram

The relative strengths of the different exchange interactions, within this crystal structure type, to get the observed

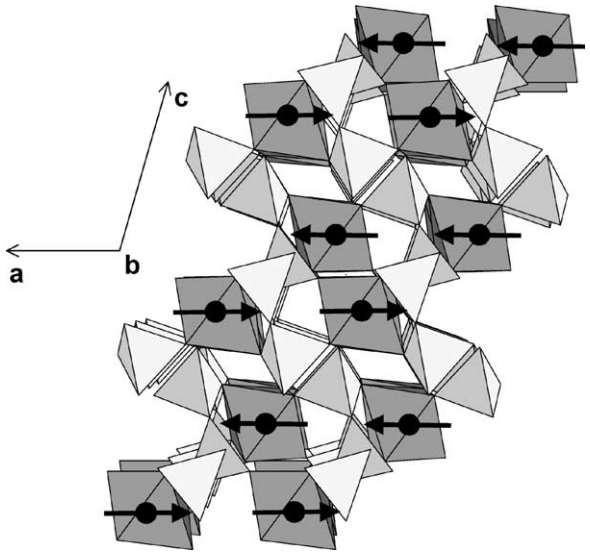

Fig. 7. Representation of the magnetic structure for $LiFeP_2O_7$. Arrows indicate the magnetic moments on the iron atoms (mostly along the a axis).

Table 2
List of $(h\,k\,l)$ reflections with their d-spacing, corresponding 2θ angle ($\lambda = 2.52$ Å), observed and calculated magnetic interaction vectors squared ($F_\perp^2 \approx I/(jLp)$) at 1.5 K in absolute units (barns/unit cell). Only reflections for $d > 3$ Å are indicated

h	k	l	Multiplicity	d (Å)	2θ	$(F_\perp)^2_{obs}$	$(F_\perp)^2_{calc}$
0	1	0	2	8.06	17.99	5.98	5.80
0	0	1	2	6.54	22.23	5.34	5.37
0	1	−1	4	5.08	28.75	0.11	0.10
1	0	0	2	4.54	32.25	0.11	0.12
1	1	−1	4	3.92	37.48	4.09	4.10
0	2	1	4	3.43	43.11	8.33	8.46
0	0	2	2	3.27	45.36	0.17	0.16
1	0	1	2	3.26	45.55	0.13	0.13
−1	0	2	2	3.20	46.33	3.02	2.96
1	1	1	4	3.02	49.35	3.26	3.25
1	2	0	4	3.01	49.45	4.29	4.26

magnetic structure as ground state, were closely examined using the two computer programs, SIMBO and ENERMAG, that are shortly described in one of our previous papers [14]. An analysis of the exchange paths leads to 3 different isotropic exchange interactions (J_i, $i = 1, 2, 3$), numbered in ascending order of distances between magnetic atoms, all of them being of super-super exchange type: two at least anions are involved in the path. We have neglected the interactions between Fe atoms separated by a distance greater than 6 Å as there is a gap (around 0.76 Å) in distances between the atoms interacting through J_3 ($d(J_3) = 5.52$ Å) and those interacting through J_4 ($d(J_4) = 6.28$ Å, well above $d(J_3)$). The exchange paths differ by changes in distances or in {(Fe–Oi–Oj), (Oi–Oj–Fe)} angles and (Fe–Oi–Oj–Fe) torsion angles (Table 3).

As already pointed out, only two iron atoms, labelled Fe1 and Fe2, are to be taken into account in the structure, the second being obtained from the first one by the symmetry

Table 3
List of effective exchange interactions considered between iron atoms and related super-super exchange paths, bond lengths and angles in $LiFeP_2O_7$. The translational part to obtain the position of the second iron atom is indicated. Labels a and b refer to the symmetry operators (x, y, z) and $(-x, y+1/2, -z)$

Interaction	Path	$d1$	$d2$	$d3$	$\alpha1$	$\alpha2$	γ	d
J_1	Fe1–O(2a)–O(1a)–Fe1 $(-1, 0, 0)$ or Fe2–O(2b)–O(1b)–Fe2 $(1, 0, 0)$	2.04	2.54	2.02	121.1	105.5	96.8	4.81
	Fe1–O(4a)–O(7a)–Fe1 $(-1, 0, 0)$ or Fe2–O(4b)–O(7b)–Fe2 $(1, 0, 0)$	1.98	2.51	1.96	107.0	133.6	113.7	4.81
J_2	Fe1–O(2a)–O(5b)–Fe2 $(-1, -1, -1)$	2.04	2.52	2.03	104.7	129.7	75.5	5.16
J_3	Fe1–O(3a)–O(7b)–Fe2 $(0, -1, 0)$	1.95	2.48	1.96	138.5	141.6	147.8	5.52

$d1 = d(\text{Fe–O}i)$, $d2 = d(\text{O}i\text{–O}j)$, $d3 = d(\text{O}j\text{–Fe})$, $\alpha1 = (\text{Fe–O}i\text{–O}j)$, $\alpha2 = (\text{O}i\text{–O}j\text{–Fe})$, $\gamma =$ torsion angle, $d = d(\text{Fe–Fe})$.

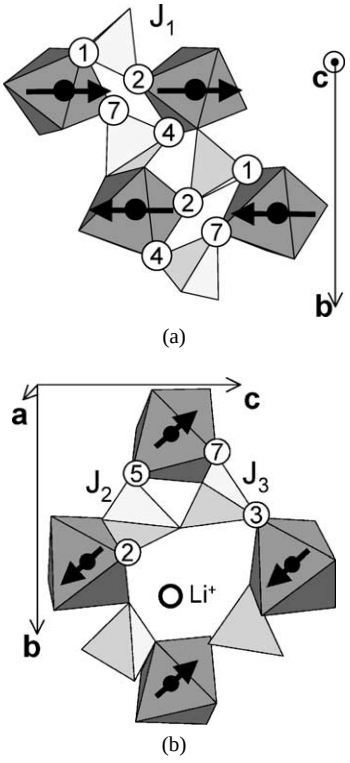

Fig. 8. Representation of three exchange paths between the iron atoms that have to be considered in $LiFeP_2O_7$. J_1 connects two translational equivalent atoms along [1 0 0] (a). J_2 and J_3 are represented in (b).

operation $(-x, y+1/2, -z)$. The exchange integral J_1, the shortest path (Fe–Fe at 4.81 Å), represents the coupling between two translational equivalent atoms along: either between two Fe1 or two Fe2 atoms, via O(1) and O(2) and via O(4) and O(7), so that this exchange path is double (Fig. 8a). The exchange integral J_2 connects Fe1 and Fe2 via O(2) and O(5); and J_3 connects Fe1 and Fe2 via O(3) and O(7). Both occur via a single exchange path in the (a, b) plane. J_2 and J_3 connect three of the four iron atoms delimiting the windows into which lithium is located, whereas J_1 is perpendicular to them: it connects iron atoms belonging to adjacent windows, in the direction of the tunnels (along [1 0 0]). Actually, there is another path connecting Fe1 and Fe2 via O(3) and O(5), with a direct Fe–Fe distance similar of that of J_2, but for which the two oxygen atoms do not belong to the same PO_4 tetrahedron, leading to a very weak contribution. J_2 and J_3 are represented on Fig. 8b.

We have calculated the phase diagram for the topology of this structural type and we can place on it the region (relative strengths and signs of the exchange interactions) corresponding to the observed magnetic structure as the ground state. The problem of the magnetic ground state of a system of classical spins connected by isotropic exchange interactions was considered 40 years ago by several authors [15–18]. Here we follow the discussion summarized in the paper of Freiser [18]. The first ordered state can be obtained from the resolution of an eigenvalue problem where the matrix is the Fourier transform of the exchange interactions. In our case there is no magnetic transition below T_N, so that the first ordered magnetic state is the ground state. We will use then the method discussed in [15,18] to evaluate the conditions satisfied by the exchange integrals in order to have the propagation vector $\mathbf{k} = (0, 0, 0)$ and the observed antiferromagnetic spin arrangement as the ground state.

The first ordered state is obtained, as a function of $\mathbf{k}$ (on the surface or at the interior of the Brillouin zone) and the exchange integrals, as the eigenvector corresponding to the lowest eigenvalue of the negative Fourier transform of exchange integral matrix [14]:

$$\xi_{ij}(\mathbf{k}) = -\sum_m J_{ij}(\mathbf{R}_m)\exp\{-2\pi i\mathbf{k}\mathbf{R}_m\}.$$

The indices i, j refer to the magnetic atoms in a primitive cell, $J_{ij}(\mathbf{R}_m)$ is the isotropic exchange interaction (including the modules of the spins) between the spins of atoms i and j in unit cells separated by the lattice vector $\mathbf{R}_m$.

In our case we have only two atoms per primitive cell, so that the above matrix is very simple and the problem can be solved analytically. The elements of the Hermitian exchange matrix $\xi_{ij}(\mathbf{k})$ are:

$$\xi_{11}(\mathbf{k}) = \xi_{22}(\mathbf{k}) = -2J_1\cos 2\pi X,$$
$$\xi_{12}(\mathbf{k}) = \xi_{21}^*(\mathbf{k}) = -\left(1 + e^{2\pi iY}\right)\left(J_3 + J_2 e^{2\pi i(X+Z)}\right).$$

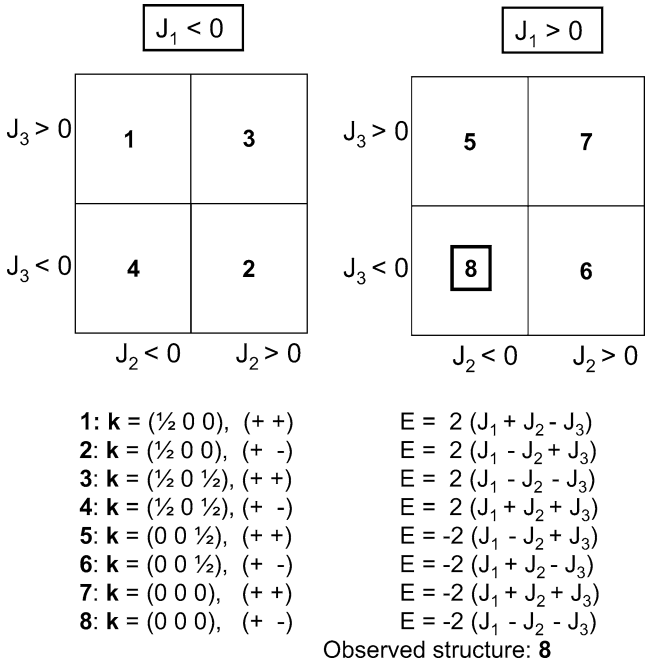

Fig. 9. Magnetic phase diagram for $LiFeP_2O_7$. The observed magnetic structure, $\mathbf{k} = (0, 0, 0)$ $(+-)$, is observed as ground state if $J_1 > 0$, $J_2 < 0$ and $J_3 < 0$. The energy, per unit cell and S^2, of each configuration is written.

The eigenvalues of this matrix are easily obtained:

$$\lambda_{1,2}(\mathbf{k}, J_1, J_2, J_3) = -2J_1 \cos 2\pi X \pm \left[2(1+\cos 2\pi Y) \times \left\{J_2^2 + J_3^2 + 2J_2J_3 \cos 2\pi(X+Z)\right\}\right]^{1/2}.$$

The conditions to get the possible stable magnetic structures are obtained putting to zero the derivatives of the eigenvalues with respect to the components of **k** and forcing the Hessian to be definite positive. Doing this work by hand is, in general, quite cumbersome so we used the program ENERMAG [14], varying the values of all the exchange interactions J_i $(i = 1, 2, 3)$ in the interval $[-10, 10]$. Only relative values are important of our purposes. The **k**-vectors were varied inside the Brillouin zone and in special points. An auxiliary program takes the output of ENERMAG and plots a high-dimensional phase diagram using the exchange interactions as Cartesian axes. The different regions correspond to different magnetic structures. An analysis of the diagram gives us immediately the conditions that the exchange integrals have to satisfy to give, as the first ordered state, the observed magnetic structure. There are only eight stable possible magnetic structures for the topology of $LiFeP_2O_7$ using up to 3 exchange integrals, each of them occupies a particular octant in the $\{J_1, J_2, J_3\}$ space. The complete phase diagram is shown in Fig. 9, with the corresponding propagation vector and the sign of the magnetic moments. The energy of each configuration is also reported. Two domains (numbered 7 and 8) with $\mathbf{k} = (0, 0, 0)$ are found, leading to the two possible collinear structures: the pure ferromagnetic one labelled as $(++)$ and the pure antiferromagnetic one $(+-)$, which is the structure effectively observed in neutron diffraction. The conditions to obtain the observed structure as ground state are very simple: $J_1 > 0$ and $J_2 < 0$ and $J_3 < 0$.

4. Conclusion

The lithium iron diphosphate $LiFeP_2O_7$ presents a magnetic phase transition at 22 K, that we have studied by means of neutron diffraction and using symmetry analysis. The magnetic moments of the two iron atoms in the unit cell are oriented antiparallel nearly along x. Three super-super exchange interactions are to be considered to obtain this magnetic structure as the ground state. The calculated magnetic phase diagram indicates that the exchange interaction along the shortest Fe–Fe distance has to be positive and the two others negative.

References

[1] A. Durif, Crystal Chemistry of Condensed Phosphates, Plenum Press, New York, 1995.
[2] K.H. Lii, Y.P. Wang, Y.B. Chen, S.L. Wang, J. Solid State Chem. 86 (1990) 143.
[3] D. Riou, N. Nguyen, R. Benloucif, B. Raveau, Mater. Res. Bull. 25 (1990) 1363.
[4] A.K. Padhi, K.S. Nanjundaswamy, C. Masquelier, J.B. Goodenough, J. Electrochem. Soc. 144 (1997) 2581.
[5] C. Wurm, M. Morcrette, G. Rousse, L. Dupont, C. Masquelier, Chem. Mater., 2002, in press.
[6] R.C. Mercader, L. Terminiello, G.J. Long, D.G. Reichel, K. Dickhaus, R. Zysler, R. Dsanchez, M. Tovar, Phys. Rev. B 42 (1) (1990) 25.
[7] T. Moya-Pizarro, R. Salmon, L. Fournes, G. Le Flem, B. Wanklyn, P. Hagenmuller, J. Solid State Chem. 53 (1984) 387.
[8] J.L. Soubeyroux, R. Salmon, L. Fournes, G. Le Flem, Physica B 136 (1986) 447.
[9] J. Belkouch, L. Monceaux, E. Bordes, P. Courtine, Mater. Res. Bull. 30 (2) (1995) 149.
[10] J. Rodríguez-Carvajal, Physica B 19 (1993) 55, see, http://www-llb.cea.fr/fullweb/powder.htm.
[11] H.M. Rietveld, J. Appl. Crystallogr. 2 (1969) 65.
[12] E.F. Bertaut, J. Phys. 32 (1971) C1.
[13] J. Rossat-Mignot, Magnetic Structures and Neutron Diffraction, Academic Press, 1987.
[14] N. El Khayati, R. Cherkaoui El Moursli, J. Rodríguez-Carvajal, G. André, N. Blanchard, F. Bouree, G. Collin, T. Roisnel, Eur. Phys. J. B 22 (4) (2001) 429.
[15] A. Yoshimori, J. Phys. Soc. Jpn. 14 (1959) 807.
[16] J. Villain, J. Phys. Chem. Solids 11 (1959) 303.
[17] D.H. Lyons, T. Kaplan, Phys. Rev. 120 (1960) 1580.
[18] M. Freiser, Phys. Rev. 123 (1961) 2003.